New insights into the ~74 ka Toba eruption from sulfur isotopes of polar ice cores

Laura Crick[1], Andrea Burke[1], William Hutchison[1], Mika Kohno[2], Kathryn A. Moore[3], Joel Savarino[4], Emily A. Doyle[5], Sue Mahony[6], Sepp Kipfstuhl[7], James W. B. Rae[1], Robert C. J. Steele[1], R. Stephen J.
5 Sparks[6] and Eric W. Wolff[5]

[1]School Of Earth And Environmental Sciences, University Of St Andrews, United Kingdom
[2]Geoscience Center (GZG), Department of Geochemistry, Georg August Universität Göttingen, Germany
[3]Department Of Atmospheric Science, Colorado State University, USA
[4]Institut Des Géosciences De L'environnement, Grenoble, France
10 [5]Department Of Earth Sciences, University Of Cambridge, United Kingdom
[6]School Of Earth Sciences, University Of Bristol, United Kingdom
[7]Alfred-Wegener-Institute, Bremerhaven, Germany

Correspondence: Laura Crick (lc258@standrews.ac.uk)

15 **Abstract.** The ~74 ka Toba eruption was one of the largest volcanic events of the Quaternary. There is much interest in determining the impact of such a huge event, particularly on the climate and hominid populations at the time. Although the Toba eruption has been identified in both land and marine archives as the Youngest Toba Tuff, its precise place in the ice core record is ambiguous. Multiple volcanic sulfate signals have been identified in both Antarctic and Greenland ice cores within the uncertainty of age estimates as possible events for the Toba eruption. We measure sulfur isotope compositions in Antarctic
20 ice samples at high temporal resolution across 11 of these potential Toba sulfate peaks in two cores to identify candidates with sulfur mass-independent fractionation (S-MIF), indicative of an eruption whose plume reached altitudes at or above the ozone layer in the stratosphere. Using this method, we identify several candidate sulfate peaks that contain stratospheric sulfur. We further narrow down potential candidates based on the isotope signatures by identifying sulfate peaks that are due to a volcanic event at tropical latitudes. In one of these sulfate peaks at 73.67 ka, we find the largest ever reported magnitude of S-MIF in
25 volcanic sulfate in polar ice, with a $\Delta^{33}S$ value of -4.75‰. As there is a positive correlation between the magnitude of the S-MIF signal recorded in ice cores and eruptive plume height, this could be a likely candidate for the Toba supereruption, with a plume height in excess of 45 km. These results support the 73.7 ± 0.3 ka (1σ) ka Ar/Ar age estimate for the eruption, with ice core ages of our candidates with the largest magnitude S-MIF at 73.67 and 73.74 ka. Finally, since these candidate eruptions occurred on the transition into Greenland Stadial 20, the relative timing suggests that Toba was not the trigger for the large
30 Northern Hemisphere cooling at this time although we cannot rule out an amplifying effect.

Climate
of the Past
Discussions

1 Introduction

The Toba caldera is located in northern Sumatra (Indonesia) and contains the largest volcanic lake on Earth. The 100 x 30 km caldera marks the location of a supereruption which occurred around 74 ka and covered most of North Sumatra in ignimbrite

35 (Chesner, 2012). Evidence for this eruption comes in the form of ash in marine cores from the Bay of Bengal, Indian Ocean, and South China Sea. On land, layers of ash in India, Malaysia, and as far as Lake Malawi in East Africa have been identified as the Youngest Toba Tuff (YTT) (Williams, 2012; Petraglia et al., 2012; Lane et al., 2013). In total, an area of ~40 million km^2 is estimated to have been covered in >5mm of ash (Costa et al., 2016). The Toba eruption is estimated to be 2 orders of magnitude greater than the 1815 Tambora eruption (Chesner et al., 1991) making it of one of the largest eruptions of the

40 Quaternary. Given the scale of the Toba eruption, there is great interest in determining the climate forcing associated with the Toba event and its timing for use as a stratigraphic marker (Oppenheimer, 2002).

Understanding the amount and height of sulfur ejected during a volcanic event is key to establishing the climatic impacts of an eruption. Volcanic eruptions release SO_2 and H_2S into the atmosphere which is rapidly oxidised to sulfate. Sulfate aerosols

45 scatter incoming solar radiation leading to cooling of the Earth's surface (Cole-Dai, 2010). In the troposphere, sulfur compounds are oxidised and precipitated out in days to weeks (Shaheen et al., 2013), whereas sulfate aerosols can remain in the stratosphere for months or years, leading to extensive global cooling (Toohey et al., 2019; Robock, 2000). For the Toba eruption, some studies have linked this event to a bottleneck in human evolution (Rampino and Ambrose, 2000) while others suggest that human evolution was mostly unaffected by the supereruption (Clarkson et al., 2020; Lane et al., 2013; Smith et

50 al., 2018). Key to unravelling its potential for climatic forcing is determining the stratospheric sulfate loading associated with this event and its precise timing.

There are currently a number of estimates for the amount of sulfur erupted into the atmosphere during the Toba event and a large range have been used to model the potential climatic impact of Toba (Yost et al., 2018). A study using melt inclusions

55 in the YTT estimate the sulfur aerosol load to be 33 Tg S (Chesner and Luhr, 2010). Subsequently, Costa et al., (2014) used the same melt inclusion data, with a different set of initial assumptions, and new estimates of the volume of the eruption to re-estimate the sulfur loading of Toba to be 850–1750 Tg S. These differences in estimates of aerosol load highlight how differences in assumptions can lead to large uncertainties associated with this technique. Furthermore, these petrological estimates can only constrain total sulfur emitted, with no distinction on how much reached the stratosphere which is crucial

60 for understanding the potential climatic impact.

An alternative means of estimating sulfur emissions from past volcanic eruptions is through analysis of sulfate from polar ice cores. Sulfate concentration measurements are available from both hemispheres with records extending back to 110 ka for Greenland (Bigler, 2004) and 800 ka for Antarctica (Wolff et al., 2010a). Peaks in sulfate concentration above background

65   concentrations can be identified as volcanic events. Large, low-latitude eruptions can distribute sulfate globally, depositing at

both poles, resulting in a coincident bipolar peak in sulfate (Sigl et al., 2013; Gao et al., 2007; Zielinski, 2000). Zielinski et al.,

(1996) identified the largest sulfate peak around the time of Toba in the GISP2 Greenland ice core, T1 in this study, and used

this to estimate a sulfur loading of 230–1140 Tg S. This range lies between the two melt inclusion estimates described above

and overlaps the upper estimate.

70

A further benefit to using ice core estimates of sulfur loading is that the isotopic composition of the volcanic sulfate deposited

in ice cores can be used to determine if the sulfate was injected into the stratosphere to altitudes at or above the ozone layer

(e.g. Savarino et al., 2003; Baroni et al., 2007; Gautier et al., 2019).Most chemical and physical processes fractionate isotopes

as a function of their masses. A notable exception is when sulfur dioxide is exposed to UV radiation it acquires a sulfur mass

75   independent fractionation (S-MIF) signature in the form of non-zero $\Delta^{33}S$ values (Savarino et al., 2003) here:

$$\Delta^{33}S = \delta^{33}S - (\delta^{34}S+1)^{0.515} +1 \qquad\qquad (1)$$

where 0.515 is the equilibrium fractionation factor given by the ratio of the differences in the reduced masses and $\delta^{x}S$ is

$$\delta\ ^{x}S = \frac{(^{x}S/^{32}S)_{sample}}{(^{x}S/^{32}S)_{reference}} -1 \qquad\qquad (2)$$

and x = 33 or 34 with Vienna-Canyon Diablo Troilite (V-CDT) as the reference.

80

In the modern atmosphere, the ozone layer prevents the relevant wavelengths in the UV spectrum from reaching the Earth's

surface. Therefore any volcanic SO_2 erupted below the ozone layer will fall along the terrestrial mass-dependent fractionation

line, but an eruption into or above the ozone layer will inherit a S-MIF signal of non-zero $\Delta^{33}S$ (Savarino et al., 2003). As the

ozone layer is in the lower stratosphere, the presence of S-MIF in volcanic sulfate can identify stratospheric sulfate. Sulfur

85   isotope compositions in volcanic sulfate from snow pits and ice cores have been measured on many of the major eruptions

within the last 2600 years (e.g. Savarino et al., 2003; Baroni et al., 2007; Cole-Dai et al., 2009; Gautier et al., 2019). This

isotope signal varies across the duration of an eruption with a number of these studies having shown that the $\Delta^{33}S$ evolves from

positive to negative values (e.g. Baroni et al., 2007; Cole-Dai et al., 2009; Burke et al., 2019). A new method of measuring ice

core sulfur isotopes by multi-collector inductively coupled plasma mass spectrometry (MC-ICPMS) (Burke et al., 2019) has

90   reduced sample size requirements by three orders of magnitude and allows us to investigate eruptions further back in the

geological record (McConnell et al., 2017).

Sulfur isotopes can also give insights into the locations of volcanic sources. Local, high latitude, stratospheric eruptions will

also deposit a large volume of tropospheric sulfur with $\Delta^{33}S = 0$ which will mute the overall S-MIF signal preserved in the ice

95   core. However, $\delta^{34}S$ and $\delta^{33}S$ in stratospheric sulfate undergo the same fractionation process, producing a slope of 0.608, rather

than the typical terrestrial mass dependent fractionation line with a slope of 0.515 (Burke et al., 2019). This deviation in slopes

is what gives the non-zero $\Delta^{33}S$ values that are strongly correlated with $\delta^{34}S$, allowing us to distinguish between sulfate peaks containing purely stratospheric sulfate and those with a tropospheric component.

100 Determining which sulfate peak in ice cores corresponds to the Toba eruption is a challenging task (Svensson et al., 2013). The YTT has been dated using $^{40}Ar/^{39}Ar$ techniques giving ages of 75.0 ± 0.9 ka (1 σ) (Mark et al., 2014), 73.88 ± 0.32 ka (1σ) (Storey et al., 2012) and 73.7 ± 0.3 ka (1σ) (Mark et al., 2017), with the final estimate being a recalculation of the dates from the data from Mark et al., (2014) and Storey et al., (2012). Based on these $^{40}Ar/^{39}Ar$ ages, nine bipolar peaks in sulfate concentration were identified in ice cores within the age uncertainties (Fig. 1; Svensson et al., 2013). These bipolar volcanic
105 ties were correlated between cores in both hemispheres by annual layer counting between the peaks in volcanic sulfate (Svensson et al., 2013).

Here we measure sulfur isotope composition of sulfate from two Antarctic ice cores for these nine Toba candidate peaks, as well as two additional sulfate peaks within the Toba $^{40}Ar/^{39}Ar$ age uncertainty window. Using these isotopic measurements we
110 can determine the injection altitude of their source eruption - stratospheric or tropospheric - and, where possible, insights into their source location (high latitude or tropical). We compare these S isotope results to ice core results from more recent eruptions over the last 2500 years to identify the most likely Toba candidate(s) and provide further constraints on the timing of the eruption and relation to other key paleoclimate records.

2 Methods

115 Ice core samples were collected from two EPICA Antarctic ice cores; Dome C (EDC) (75°06' S; 123°21' E, 3233 m), drilled from 1999–2005 and Dronning Maud Land (EDML) (75°00' S, 00°40' E, 2892 m), drilled from 2000–2006 (Severi et al., 2007). All nine of the Toba candidate peaks of varying magnitude, shown in Fig. 1, have been previously identified in both EDML (Antarctic) and NGRIP (Greenland) cores (Svensson et al., 2013, their Table 2). Five of the candidate peaks have also been identified in the EDC core sulfate record. The T4 peak is not shown in EDC on Fig. 1 as it does not have a peak in sulfate
120 concentration but it is identified by electrical conductivity measurement (Svensson et al., 2013). Samples from EDC included Toba candidates T1, T2 and T3 and an additional peak positioned between T4 and T5 (T4b). The EDML core was sampled for all nine Toba peaks identified by Svensson et al., (2013), as well as a small peak prior to T1 (Pre-T1).

Multiple samples were taken across each of these peaks and include pre-event background samples. Where possible, samples
125 containing a minimum of 20 nmol sulfate were taken, allowing for repeat isotopic measurements (c.f. Burke et al. 2019). During sampling the outside of ice samples was scraped clean to remove any potential contaminant derived from drilling fluids. Sulfate concentration of the samples was determined by ion chromatography using a Metrohm 930 Compact IC Flex using 600 μl aliquots of sample. Once the concentration of the samples was determined, the volume of sample required to give 20

Climate
of the Past
Discussions

nmol of sulfate was dried down in Savillex PFA Teflon vials on a hotplate. These volumes ranged from 14 ml for background

130 samples to 2 ml for the highest sulfate concentration samples. Once dry, samples were re-dissolved in 70 µl 0.01 % volume distilled HCl. The sulfate was then extracted from the samples using column chemistry following the procedure detailed in Burke et al., (2019). For each set of 12 samples, a secondary river water standard, Switzer Falls (Burke et al., 2018; 2019), and a total procedural blank were also put through columns for analysis. After sulfate is isolated by column chemistry, the triple sulfur isotope composition (^{32}S, ^{33}S and ^{34}S) were measured using a Neptune Plus MC-ICPMS (Paris et al., 2013; Burke et al.,

135 2019). Samples and standards were measured twice during a single analytical session, along with total procedural blanks. The reproducibility of the Switzer Falls standard over the course of this study was $\delta^{34}S = 4.15 \pm 0.15$ ‰ and $\Delta^{33}S = -0.02 \pm 0.17$ ‰ (n = 25, 2 s.d.), in agreement with ratios from previous studies of $\delta^{34}S = 4.17 \pm 0.11$ ‰ and $\Delta^{33}S = 0.01 \pm 0.10$ ‰ (Burke et al., 2018, 2019). Procedural blanks had 0.24 ± 0.12 nmol S with a $\delta^{34}S = 4.32 \pm 2.67$ ‰ (n = 18, 2 s.d.), and were used to blank correct all measured ratios.

140

Background sample(s) from immediately before the peak in volcanic sulfate were used in conjunction with concentration data to determine the fraction of volcanic sourced sulfate for each sample and the isotopic compositions of the volcanic fraction ($\delta^{34}S_{volc}$ and $\delta^{33}S_{volc}$) (following Baroni et al., 2007):

$$\delta^{x}S_{volc} = \frac{\delta^{x}S_{meas} - f_{background} \cdot \delta^{x}S_{background}}{f_{volc}} \qquad (3)$$

145 Finally, these values were used to calculate $\Delta^{33}S_{volc}$, with uncertainty propagated throughout using a Monte Carlo routine. If background samples were not available for a sulfate peak an average was taken of all background samples from the same core over the Toba time period. Unless stated, we have only considered the $\delta^{34}S_{volc}$ and $\delta^{33}S_{volc}$ from samples with volcanic fractions ≥ 65% (Burke et al., 2019; Gautier et al., 2018), as the propagated errors are prohibitively large to interpret $\delta^{34}S_{volc}$ and $\delta^{33}S_{volc}$ from samples with smaller volcanic fractions.

150 **3 Results**

Due to sulfate diffusion in the ice cores, volcanic peaks broaden and reduce in amplitude at depth (Barnes et al., 2003). To account for this diffusion effect we consider the area represented under the sulfate peaks to calculate the total deposition of sulfate for a given event (Sparks et al., in review). The background rate is calculated using the running median over 200 years centred on the peak, this integration also corrects for thinning. The deposition of sulfate for the Toba candidates range from

155 26–133 mg m^{-2} in EDC and 27–424 mg m^{-2} in EDML (Fig. 2, Table S1). In the EDC core over the last 100 ka, 335 sulfate peaks have total depositions >20 mg m^{-2}, considered to be the threshold for magnitude 6.5 or greater events (Sparks al., in review). In this ranking T3 is the 7th highest sulfate deposition (133 mg m^{-2}) in the last 100 ka. All of the other Toba candidates in EDC are ranked lower with next largest peak, T1 (54 mg m^{-2}) ranked 67th, 1 place above the 1815 CE Tambora eruption. T2 is also in the top 100 peaks with a deposition of 47 mg m^{-2}.

160

Sulfate data are not available from the top of the EDML core (Severi et al., 2007) and as such, comparisons between the Toba candidate sulfur depositions and large Common Era eruptions are not possible. However, total deposition calculations using the FIC (fast ion chromatography) data from 800 CE to 76 ka rank T2 as the highest peak by deposition (424 mg m^{-2}), followed by T4 (240 mg m^{-2}) as the 5th highest. T1 (88 mg m^{-2}), T3 (103 mg m^{-2}), T6 (96 mg m^{-2}) and T9 (86 mg m^{-2}) all rank within

165 the top 50 sulfate peaks in the core over this period.

Of the 14 peaks measured in EDC and EDML, 13 had samples with non-zero $\Delta^{33}S$ values (Fig. 2). Of all the peaks measured in this study, T1, T2, and T3 had the highest magnitude S-MIF signals (<-0.9 ‰). All of the data measured from these three peaks in both cores are plotted for comparison in Fig. 3, as well as T4 from EDML since it is also considered to be a more

170 likely Toba candidate than T5–T9 (Svensson et al., 2013; Polyak et al., 2017). Results for the other Toba peaks measured in this study are shown in supplementary figures S1–6.

T1 in EDC shows a large decrease in volcanic $\delta^{34}S$ to -48.2 ‰. A negative volcanic $\Delta^{33}S$ of -4.75 ‰ was also measured in the EDC T1 samples, but no positive MIF values were measured. In EDML, T1 shows a negative excursion in $\delta^{34}S_{volc}$ to -29.4 ‰.

175 Unlike the EDC samples for T1, both a positive and negative volcanic MIF excursion was measured in EDML with the $\Delta^{33}S$ signal evolving from background to +1.34 ‰ then dropping to -3.08 ‰. These are the largest magnitude volcanic MIF signals measured in this study for the Toba candidates in each of the cores.

T2 in EDC initially shows little change in measured $\delta^{34}S$ before decreasing to -13.6 ‰, with a $\delta^{34}S_{volc}$ of -21.9 ‰. The

180 background corrected data show an initial positive $\Delta^{33}S$ of +0.57 ‰, and after this the remainder of the samples record a negative MIF signal, with $\Delta^{33}S_{volc}$ falling to -3.41 ‰. The volcanic $\delta^{34}S$ and $\Delta^{33}S$ signals in EDML show a very similar evolution to their EDC counterparts with a decrease in $\delta^{34}S$ to -6.46 ‰ before returning to background levels. Both positive and negative volcanic MIF signals are recorded, increasing up to +0.74 ‰ before reducing to -1.72 ‰.

185 The measured $\delta^{34}S$ from T3 in EDC decreases from a background value of +16.3 ‰ to -0.8 ‰ before returning to +16.1 ‰. The volcanic MIF evolution follows a trend from positive (+0.62 ‰) to negative (-0.93 ‰). The measured $\delta^{34}S$ signal for T3 in EDML decreases from background level of +16.2 ‰ to +9.9 ‰ during the eruption before increasing again. In contrast to T3 in EDC, the EDML samples have preserved only a positive volcanic MIF signal of +0.99 ‰.

190 Of the remaining peaks, the peak prior to T1 and T4–T9 in EDML all have one or more samples with a non-zero $\Delta^{33}S$, though smaller in magnitude than measured in T1, T2 and T3 (see Table S1and figures S1–6). The additional peak between T4 and T5 sampled from EDC had the lowest sulfate deposition of the Toba candidates in the sampled peaks from EDC at 26 mg m^{-2}. This is the only peak in this study where all samples had $\Delta^{33}S$ values within 2σ of 0 ‰.

Climate
of the Past
Discussions

4 Discussion

195 ### 4.1 Preservation of S-MIF in Toba candidate events from two Antarctic ice cores

The presence of non-zero $\Delta^{33}S$ (beyond typical ± 0.17 ‰ uncertainty, see *Methods*) in volcanic sulfate from ice cores suggests that the sulfate deposited from these eruptions came from the stratosphere at altitudes at or above the ozone layer where it could interact with UV radiation (Savarino et al., 2003). Of the 14 Toba candidates measured in this study across both EDC and EDML cores, 13 showed a non-zero stratospheric MIF signal (Fig. 2). The only event that had a zero S-MIF was the small

200 peak between T4 and T5 sampled in EDC. This result suggests that the sulfur associated with this volcanic eruption did not make it as high as the ozone layer and it was likely a local eruption, which could also account for the lack of a corresponding sulfate peak in EDML (Fig. 1).

For the three peaks that were measured in both EDC and EDML (T1–3), there is good agreement in the S isotope records

205 between the two cores (see Fig. 3). The main difference is that the EDC $\delta^{34}S$ and $\Delta^{33}S$ are consistently more negative than those measured in EDML. This could be due to an increased influence of marine sulfate ($\delta^{34}S$ ~20‰, Paris et al., 2013) at EDML that is not adequately accounted for in the background correction, which could be influenced by factors such as diffusion. There are also slight differences between the cores in the preservation of the positive or negative S-MIF across individual events. For example, only the negative S-MIF signature is preserved in T1 in EDC, and only the positive S-MIF

210 signature is preserved in T3 in EDML, whereas T1 in EDML and T3 in EDC show both positive and negative S-MIF. Previous studies that have measured S isotopes in multiple samples across a volcanic sulfate peak in ice or snow have shown that the $\Delta^{33}S$ evolves from positive to negative values (e.g. Baroni et al., 2007; Cole-Dai et al., 2009; Burke et al., 2019). Thus, the initial sulfate that is deposited on ice sheets following a volcanic eruption inherits a positive S-MIF signal in the stratosphere, and this sulfate is isolated (in time or space) from the residual sulfate that is deposited later with a negative S-MIF signature

215 (Baroni et al., 2007; Gautier et al., 2018). Mass balance should require that the sum of the positive and negative anomalies should balance out. However, at low accumulation rate sites cores, such as Dome C, occasionally only the positive or negative component is preserved (Gautier et al., 2018, 2019). This loss of a proportion of the sulfate is perhaps not surprising in these cores given that at low accumulations sites like Dome C, entire sulfate peaks (such as the 1815 Tambora eruption) might be missing from an individual core (Gautier et al., 2016). Given that some volcanic sulfate may not be preserved in these Toba

220 candidate events, and that sulfate diffuses in the ice cores, the isotope compositions measured in the Toba candidate peaks should be viewed as minimum magnitude $\Delta^{33}S$ values. Due to the low accumulation rate at Dome C the calculated sulfate depositions are minimum estimates.

As most of the Toba candidates measured in the cores have a stratospheric S-MIF signal, the Toba eruption cannot be

225 immediately identified purely on the presence or absence of S-MIF. However, recent work by Lin et al., (2018) shows a correlation between $\Delta^{33}S$ and cosmogenic ^{35}S in modern aerosols which suggests that sulfate formed at higher altitudes has a

greater positive Δ^{33}S. Although the exact photochemical process that imparts the S-MIF is not fully understood (see e.g. Gautier et al., (2018) for a discussion), the relationship between altitude and Δ^{33}S implies that the magnitude of the Δ^{33}S recorded in ice cores should scale with a volcanic eruption's plume height. Due to isotopic mass balance, the large negative Δ^{33}S signals

230   measured for T1 and T2 in EDC would also have a complementary large positive Δ^{33}S signal which was not deposited and preserved due to the low accumulation at the site. In turn, these large positive signals would be indicative of exceptionally large volcanic plume heights.

We can further narrow down potential Toba candidates by considering the δ^{34}S signal measured across these events as well.

235   Given the low latitude location of the Toba caldera, any sulfate deposited in Antarctica from the Toba eruption would have to be delivered via the stratosphere from heights at or above the ozone layer. Due to the difference in δ^{34}S vs δ^{33}S slope from stratospheric and terrestrial sulfate (0.608 vs 0.515 respectively), non-zero Δ^{33}S in stratospheric sulfate is strongly correlated with δ^{34}S (Burke et al., 2019). In contrast, if some tropospheric sulfate is present in the ice core, for example from a stratospheric, extratropical eruption proximal to Antarctica, the sulfur isotope compositions measured in ice would not exhibit

240   a strong positive correlation between Δ^{33}S and δ^{34}S, since Δ^{33}S in this tropospheric sulfate would be zero, and its δ^{34}S value would reflect the isotopic composition of the erupted sulfur gases (Burke et al., 2019). Indeed, for the extratropical eruption of Katmai/Novarupta (Alaska) in 1912, the sulfur isotope compositions measured in Greenland showed a weak negative correlation between Δ^{33}S and δ^{34}S (Burke et al., 2019).

245   Of the stratospheric candidates, T1, T2 and T3 all show a strong positive correlation between δ^{34}S and Δ^{33}S in both cores suggesting that the sulfate comprising these peaks was purely stratospheric in origin. This suggests they are most likely to be from a tropical eruptions source and therefore are the best candidates for the Toba eruption. It should be noted however that these sulfate peaks could also have been deposited by an extratropical event with a low tropospheric sulfur load. Overall, the linear regression (York et al., 2004) for these three events in two cores gives a slope of 0.106 ± 0.003 (1σ) with an r^2 value of

250   0.964, and similar to the slopes reported by Gautier et al (2018) of 0.09 ± 0.02 and Burke et al (2019) of 0.089 ± 0.003 for tropical eruptions measured in ice cores (Fig. 4a).

The remaining Toba candidates either did not have multiple samples with enough volcanic sulfate ($f_{volc} \geq 0.65$) to investigate correlations (Pre-T1, T5, T7, T8, T9) or they did not show strong positive correlations between δ^{34}S and Δ^{33}S (T4 and T6).

255   Both T4 and T6 in EDML have only weak statistical correlations between δ^{34}S and Δ^{33}S with slopes of 0.081 ± 0.063 and 0.037 ± 0.018 respectively with weighted r^2 values of 0.088 (T4) and 0.065 (T6). This indicates that a substantial proportion of the sulfate deposited on the ice sheet originated from below the ozone layer. Given the presence of MIF in both of these sulfate layers, we can conclude that the eruptions were large enough to reach the stratosphere at or above the ozone layer, but likely they were extratropical. In the case of T4, this could in part help to explain why this sulfate peak is not obviously

260   apparent in EDC if a large portion of the sulfate in EDML was deposited directly via the upper troposphere/lower stratosphere.

Climate
of the Past
Discussions

Although it is possible for large extratropical eruptions to deposit sulfate at both poles (Baines et al., 2008; Toohey et al., 2016) the bipolar attribution of T4 and T6 (and associated chronological constraints on ice core age models) should be investigated further for these events by analysing high resolution sulfur isotope compositions from Greenland ice cores.

4.2 Comparison to eruptions over the Common Era

265 Sulfur mass independent fractionation in ice core sulfate has been measured in numerous volcanic events over the last 2600 years (Fig. 5, Savarino et al., 2003; Baroni et al., 2007; Baroni et al., 2008; Cole-Dai et al., 2009; Gautier et al., 2018; Burke et al., 2019; Gautier et al., 2019). The negative S-MIF signals measured in T1 and T2 are the largest magnitude volcanic S-MIF signals, and in T1 in EDC has the most negative $\Delta^{33}S$ value (-4.75‰) recorded in ice core sulfate (Fig. 5).

270 If the magnitude of the S-MIF signal scales with altitude as suggested by Lin et al., (2018), then the results from the T1 Toba candidate would suggest that this eruption had a plume that reached higher altitudes than other eruptions that occurred over the last 2.6 ka (Gautier et al., 2019), making it a good candidate for the Toba eruption which is thought to be one of the largest eruptions of the last 100 ka (Rougier et al., 2018).

275 For further comparison to Common Era eruptions, we compared the total sulfate deposition in EDC for T1, T2 and T3 (see Fig. 2a) to the sulfate deposition of major eruptions in the Common Era in both EDC and globally. In the EDC core we find that the T1 and T2 sulfate deposition, 54 and 47 mg m^{-2} respectively, is of a similar sulfur loading to that of the 1815 Tambora eruption (53 mg m^{-2}) which is in agreement with the low estimates of sulfur loading from melt inclusion data from Chesner and Luhr, (2010). However, as Dome C is a low accumulation site, we also consider the total deposition to both Antarctica 280 and Greenland from the Toba candidates. This is achieved by first comparing the deposition from Common Era eruptions in the EDC ice core record to the calculated total Antarctic deposition for the same Common Era events from the compilation of Antarctic cores in Sigl et al., (2015). The correlation ($r^2 = 0.71$; Fig. S7) between these deposition masses suggests we can use this relationship to scale the EDC sulfate deposition of the Toba candidates to approximate a total Antarctic deposition for these events. We have used sulfate concentration data for NGRIP from Svensson et al., (2013) and accumulation data from 285 Kindler et al., (2014) to determine the sulfate deposition for T1, T2 and T3 in the NGRIP core. This is subsequently scaled to a total deposition over Greenland using the relationship established by Toohey and Sigl, (2017). These total depositions over Greenland and Antarctica are used to calculate the stratospheric sulfur loading following the method detailed in Toohey and Sigl, (2017). Scaling the sulfate flux in this manner, we calculate stratospheric sulfur loadings of 148, 176 and 73 Tg S for T1, T2 and T3 respectively, all of which are greater than the stratospheric loadings due to the 1257 Samalas eruption of 59.4 Tg S 290 (Toohey and Sigl, 2017).

These sulfur emissions fall within the broad range of estimates of sulfur loading for the Toba eruption (e.g. 33–1750 Tg from petrological and volume estimates (Chesner and Luhr, 2010; Costa et al., 2014) and previous ice core estimates of T1 (Zielinski

9

295   et al., 1996)), but are on the lower range of estimates. These results suggest that either there is an incorrect assumption in the scaling of revised erupted volume calculations leading to the large estimates of 850–1750 Tg S (Costa et al., 2014) or a large portion of the erupted sulfur either did not make it into the stratosphere or it was rapidly removed. Both scenarios suggest that despite the massive erupted volume associated with the YTT eruption, the stratospheric sulfate loading was not orders of magnitude larger than more recent eruptions within the Common Era, but may have still been 2–3 times greater than that of the 1257 Samalas eruption.

300   **4.3 Toba eruption dynamics**

The atmospheric sulfur loading from an eruption depends on the eruption dynamics. Caldera forming eruptions can often erupt in two phases. The first phase is a Plinian eruption from a single vent producing a high, buoyant plume. Then when the cone collapses, multiple vents can form leading to pyroclastic flows and co-ignimbrite plumes (Wilson, 2008). In the case of Toba the marine ash layer in the Indian Ocean displays a coarse lower layer and a fine grained upper layer (Ninkovich et al., 1978).

305   The lower layer was interpreted by Ninkovich et al (1978) as a Plinian deposit, but no basal Plinian deposit has been yet identified beneath the ignimbrite surrounding Toba caldera leading the interpretation that the distal ash deposits are co-ignimbrite in origin (Chesner, 2012). Co-ignimbrite plumes can transport sulfur compounds into the stratosphere and can reach plume altitudes similar to Plinian plumes (Engwell et al., 2016) and deposit ash over a wide area (Chesner, 2012). In addition, over-plumes forming above the main plume for events on the scale of Toba could potentially extend the total plume height to

310   ~60–70 km (Costa et al., 2018).

The Toba ash fall deposit is consistent with an exceptional plume height in two ways (Ninkovich et al., 1978; Liang et al., 2001). First is the large area of ash dispersal covering much of the northern Indian Ocean and Indian sub-continent and as far as East Africa in the west and extending to the South China Sea to the north east (Lane et al., 2013). Second is the exceptional

315   coarse grain size of the Toba deposit which has a median grain size about 8 times greater than the tephra deposits of Tambora 1815 and the Late Bronze Age Santorini tephra deposits at about 500 km from source (Ninkovich et al., 1978; Kandlbauer et al., 2013) and 2.5 times greater than the Campanian tephra deposits at about 1700 km from source (Engwell et al., 2014). These features can be explained by a giant eruption cloud of exceptional size. The height of the Toba plume can be constrained by modelling (c.f. Baines and Sparks, 2005; Costa et al., 2014). These results indicate cloud heights exceeding 40 km, although

320   these estimates should be caveated by the large uncertainties in the input parameters, such as eruption duration (Oppenheimer, 2002). This exceptionally large eruption and plume height is reflected in the sulfur isotope compositions. For example, T1 and T2 in both EDC and EDML preserve large magnitude S-MIF signals, the magnitude of which may correlate with altitude as suggested by Lin et al., (2018).

325   Independent geological estimates of eruption plume height are available for numerous Common Era eruptions, determined by a range of methods including using cloud positions from satellite sensors (Guo et al., 2004) and modelling lithic clast dispersal

(Sigurdsson and Carey, 1989). A comparison of these Common Era eruption plume heights and high resolution (≥5 samples/peak) S isotope measurements from ice cores (Burke et al., 2019) or snow pits (Baroni et al., 2007) suggests a positive correlation between the maximum $\Delta^{33}S$ value measured and plume height (Fig. 6). If this relationship is extrapolated to the

330   range of MIF signals measured for T1 and T2, we would anticipate the plume height to be in excess of 45 km, similar to the model estimate of ~ 42 km from Costa et al., (2014). However, this estimate is based on a tentative relationship between $\Delta^{33}S$ and plume height from only a handful of Common Era eruptions, and thus should be further investigated and validated. One such method that could provide additional information on plume height is sulfate oxygen MIF measurements ($\Delta^{17}O$), since O-MIF in OH in the stratosphere varies with altitude (Zahn et al., 2006) which can then be inherited by sulfate during oxidation

335   (Gautier et al., 2019).

Using annual layer counting, T1 and T2 are separated by ~80–90 years in the ice core record (Svensson et al., 2013). Given this close spacing and the large negative S-MIF signals for both peaks, there is an alternative interpretation that T1 and T2 and possibly even T3 are all pulses of the YTT. Such an interpretation is supported by recent research on comparable supereruptions

340   which indicate that these eruptions can be more complex multi-episode events. The Huckleberry Tuff erupted from Yellowstone caldera is a comparable magnitude eruption to Toba and detailed field studies (Swallow et al., 2019) show that there were three episodes with gaps of weeks to months occurred between the first two episodes, and years to decades between the second two. The explanation of multiple pulses reflects the disturbance of multiple spatially separated magma chambers. Petrological and geochemical evidence for supereruptions disturbing multiple chambers, involving magma assemble for such

345   eruptions over decades to centuries having more complex prolonged eruptive histories is emerging in other examples (Druitt et al., 2012; Shamloo and Till, 2019). Thus the assumption that such Toba and Yellowstone magnitude eruptions are single geologically instantaneous events may be wrong and opens up the option of assigning multiple closely spaced sulfate peaks to Toba.

350   **4.4 Impact and timing of the Toba eruption**

Given the scale of the Toba event, we consider the potential impact of the eruption on global climate. Over the last ice age, millennial duration cycles of abrupt changes in climate in the Northern Hemisphere are recorded in paleoclimate records (Broecker, 2000). The estimated dates for the Toba eruption coincide with the transition into one of these cold periods, Greenland Stadial 20 (GS-20); however it is unclear as to whether the Toba eruption caused this Northern Hemisphere cooling

355   or if it was already underway (Baldini et al., 2015).

Our data allow us to narrow down the Toba candidates and hence the timing of the eruption and its relationship to GS-20. As T1 and T2 show the largest magnitude S-MIF signals we consider them to be the best candidates for the Toba eruption, which

Climate
of the Past
Discussions

places them on the transition into GS-20 (see Fig. 7 below; Svensson et al., 2013). This relative timing implies that the Toba

360   eruption was not a trigger for the Northern Hemisphere cooling.

We can also use the ice core records to put further constraints on the timing of the Toba eruption. There are two potential age
models for NGRIP records over this time interval: GICC05modelext (Wolff et al., 2010b) and AICC2012 (Veres et al., 2013).
Although the GICC05modelext and AICC2012 timescales are the same over the last 60.2 ka, the transitions between stadial
and interstadial climate can differ on the two age scales by of a couple of millennia by 100 ka (Veres et al., 2013). Since the

365   AICC2012 age model takes into consideration the volcanic bipolar synchronization over this particular time period from
Svensson et al., (2013), studies that compare records from both hemispheres are encouraged to use the AICC2012 age model
to not introduce any artificial leads and lags in records, whereas the GICC05modelext continues to be used when considering
only Greenland records. These differences in age models put T1 and T2 in NGRIP at 74.06 and 74.16 ka on the

370   GICC05modelext, and 73.66 and 73.75 ka on the AICC2012 age model respectively.

While these differences in ages between the two age models are well within the uncertainties of the ice core age models around
this time (~1500 years, Veres et al., 2013), we can further improve on the estimates of the absolute age of the T1 and T2 events
through comparison of the Greenland $\delta^{18}O$ records with speleothem records of the Asian monsoon (e.g. Wang et al., 2001;

375   Chen et al., 2016; Du et al., 2019). Speleothems can be radiometrically dated using U-Th techniques with uncertainties of <200
years around this time (Du et al., 2019), and a systematic analysis of the timing of transitions out of stadial events in Greenland
and weak monsoon events recorded in speleothems over the past 45 ka has shown these transitions are synchronous within
189 years (Adolphi et al., 2018). Previous work has used this correlation between Greenland $\delta^{18}O$ records and speleothem $\delta^{18}O$
records with change point analysis to investigate the timing of Toba candidates (Du et al., 2019).

380

Using a record of $\delta^{18}O$ from Yangkou which has the highest resolution $\delta^{18}O$ and best age control over this time period, Du et
al. suggested a shift in the GICC05modelext by 150 years. However, because the duration of the Greenland stadial is 260 years
longer than the duration of weak monsoon event (1760 years v 1500 years respectively, determined using the NGRIP depths
and ages from Rasmussen et al., 2014), choosing whether to apply the change point analysis to the initiation of GS-20 or the

385   initiation of the Greenland Interstadial 19 impacts the estimated ages of the Toba candidate events (Du et al., 2019). The
duration of GS-20 on the AICC2012 age model (1550 years) on the other hand is more similar to the duration of the weak
monsoon event recorded in the Yangkou's speleothem (1500 years), and both the transitions into and out of GS-20 on the
AICC2012 age model are within the ~100–200 year U-Th age uncertainty of the weak monsoon event transitions reconstructed
in the speleothem (Fig. 7). Thus, without having to apply any shifts to the AICC2012 age model, the absolute ages of the

390   NGRIP $\delta^{18}O$ record on the AICC2012 age model are consistent with the radiometrically dated speleothem over this time
interval. We can then use T1 and T2 on the AICC2012 age model to suggest revised ice core dates of our best candidates for
the Toba eruption of 73.65 and 73.77 ka BP, with an uncertainty of about 0.2 kyr based on the uncertainties from the U-Th

ages (Du et al., 2019) and any potential leads and lags in the correlation between the Greenland and the speleothems (Adolphi et al., 2018). This range of dates is in agreement with the ages for the YTT from Storey et al., (2012) (73.88 ± 0.64 ka, 2σ) and

395   Mark et al., (2017) (73.7 ± 0.6 ka, 2σ), though with smaller uncertainties.

5 Conclusions

Our data shows that distinct, large magnitude MIF signals can be preserved in volcanic ice core sulfate despite undergoing diffusion for over 70 ka. Given the large magnitude MIF signals recorded in both EDC and EDML and the positive correlation between $\Delta^{33}S_{volc}$ vs $\delta^{34}S_{volc}$, T1 and T2 are the most likely candidates for the Toba eruption. This in turn places the Toba

400   eruption between 73.65–73.77 ka, during the transition to Greenland Stadial 20. This would remove Toba as a trigger for the stadial period, although we cannot rule out a role for the eruption in amplifying the transition. Our estimates of sulfate flux deposited in both poles for these events suggest that Toba's stratospheric sulfur loading was 2–3 times greater than to that of the 1257 CE Samalas eruption.

405   Sulfur isotopic composition measurements on ice core sulfate from Greenland identified as the Toba candidates, particularly T1 and T2, would be an essential next step in further constraining the Toba eruption in the bipolar ice core record. In addition to sulfate, tephra can also be used to identify volcanic eruptions in ice cores (Abbott and Davies, 2012). Toba tephra has yet to be identified in either Greenland or Antarctic ice cores (Svensson et al., 2013) despite tephra being identified in Antarctica for other similar or smaller magnitude tropical volcanic eruptions such as Samalas (Lavigne et al., 2013). However with method

410   improvements in tephra extraction (Iverson et al., 2017; Narcisi et al., 2019) it may be possible to identify the volcanic peak(s) corresponding to Toba and further constrain the timing of the largest volcanic event of the Quaternary.

Climate
of the Past
Discussions

Author contribution

LC, EAD, and SM sampled the EDC ice cores and MK and SK sampled the EDML ice cores. AB and KAM measured S isotopes from EDML and LC measured S isotopes from EDC with supervision from AB, RCJS, and JWBR. LC and AB analysed isotope data and LC analysed sulfate concentration data, with help from EWW. LC and AB developed the initial interpretation and LC wrote the initial draft manuscript, with early contributions from AB, WH, JS, RSJS, and EWW. AB, RSJS, and MK funded the project through grants (see acknowledgements). AB supervised the project. All co-authors contributed to the writing and editing of the final submitted manuscript.

References

Abbott, P. M. and Davies, S. M.: Volcanism and the Greenland ice-cores: The tephra record, Earth-Science Rev., 115, 173–191, https://doi.org/10.1016/j.earscirev.2012.09.001, 2012.

Adolphi, F., Bronk Ramsey, C., Erhardt, T., Lawrence Edwards, R., Cheng, H., Turney, C. S. M., Cooper, A., Svensson, A., Rasmussen, S. O., Fischer, H., and Muscheler, R.: Connecting the Greenland ice-core and U/Th timescales via cosmogenic radionuclides: Testing the synchroneity of Dansgaard-Oeschger events, Clim. Past, 14, 1755–1781, https://doi.org/10.5194/cp-14-1755-2018, 2018.

Baines, P. G. and Sparks, R. S. J.: Dynamics of giant volcanic ash clouds from supervolcanic eruptions, Geophys. Res. Lett., 32, https://doi.org/10.1029/2005GL024597, 2005.

Baines, P. G., Jones, M. T., and Sparks, R. S. J.: The variation of large-magnitude volcanic ash cloud formation with source latitude, J. Geophys. Res., 113, https://doi.org/10.1029/2007JD009568, 2008.

Baldini, J. U. L., Brown, R. J., and McElwaine, J. N.: Was millennial scale climate change during the Last Glacial triggered by explosive volcanism?, Sci. Rep., 5, 1–9, https://doi.org/10.1038/srep17442, 2015.

Barnes, P. R. F., Wolff, E. W., Mader, H. M., Udisti, R., Castellano, E., and Röthlisberger, R.: Evolution of chemical peak shapes in the Dome C, Antarctica, ice core, J. Geophys. Res. D Atmos., 108, 1–14, https://doi.org/10.1029/2002jd002538, 2003.

Baroni, M., Thiemens, M. H., Delmas, R. J., and Savarino, J.: Mass-Independent Sulfur Isotopic Compositions in Stratospheric Volcanic Eruptions, Science, 315, 84–87, https://doi.org/10.1126/science.1131754, 2007.

Baroni, M., Savarino, J., Cole-Dai, J., Rai, V. K., and Thiemens, M. H.: Anomalous sulfur isotope compositions of volcanic

sulfate over the last millennium in Antarctic ice cores, J. Geophys. Res. Atmos., 113, 1–12, https://doi.org/10.1029/2008JD010185, 2008.

455   Bazin, L., Landais, A., Lemieux-Dudon, B., Toyé Mahamadou Kele, H., Veres, D., Parrenin, F., Martinerie, P., Ritz, C., Capron, E., Lipenkov, V., Loutre, M. F., Raynaud, D., Vinther, B., Svensson, A., Rasmussen, S. O., Severi, M., Blunier, T., Leuenberger, M., Fischer, H., Masson-Delmotte, V., Chappellaz, J., and Wolff, E.: An optimized multi-proxy, multi-site Antarctic ice and gas orbital chronology (AICC2012): 120-800 ka, Clim. Past, 9, 1715–1731, https://doi.org/10.5194/cp-9-1715-2013, 2013.

460   Bigler, M.: Hochauflösende Spurenstoffmessungen an polaren Eisbohrkernen: Glazio-chemische und klimatische Prozessstudien, University of Bern, Switzerland, 2004.

Broecker, W. S.: Abrupt climate change: Causal constraints provided by the paleoclimate record, Earth Sci. Rev., 51, 137–154, https://doi.org/10.1016/S0012-8252(00)00019-2, 2000.

Buizert, C., Adrian, B., Ahn, J., Albert, M., Alley, R. B., Baggenstos, D., Bauska, T. K., Bay, R. C., Bencivengo, B. B.,
465   Bentley, C. R., Brook, E. J., Chellman, N. J., Clow, G. D., Cole-Dai, J., Conway, H., Cravens, E., Cuffey, K. M., Dunbar, N. W., Edwards, J. S., Fegyveresi, J. M., Ferris, D. G., Fitzpatrick, J. J., Fudge, T. J., Gibson, C. J., Gkinis, V., Goetz, J. J., Gregory, S., Hargreaves, G. M., Iverson, N., Johnson, J. A., Jones, T. R., Kalk, M. L., Kippenhan, M. J., Koffman, B. G., Kreutz, K., Kuhl, T. W., Lebar, D. A., Lee, J. E., Marcott, S. A., Markle, B. R., Maselli, O. J., McConnell, J. R., McGwire, K. C., Mitchell, L. E., Mortensen, N. B., Neff, P. D., Nishiizumi, K., Nunn, R. M., Orsi, A. J., Pasteris, D. R., Pedro, J. B., Pettit,
470   E. C., Price, P. B., Priscu, J. C., Rhodes, R. H., Rosen, J. L., Schauer, A. J., Schoenemann, S. W., Sendelbach, P. J., Severinghaus, J. P., Shturmakov, A. J., Sigl, M., Slawny, K. R., Souney, J. M., Sowers, T. A., Spencer, M. K., Steig, E. J., Taylor, K. C., Twickler, M. S., Vaughn, B. H., Voigt, D. E., Waddington, E. D., Welten, K. C., Wendricks, A. W., White, J. W. C., Winstrup, M., Wong, G. J., and Woodruff, T. E.: Precise interpolar phasing of abrupt climate change during the last ice age, Nature, 520, 661–665, https://doi.org/10.1038/nature14401, 2015.

475   Burke, A., Present, T. M., Paris, G., Rae, E. C. M., Sandilands, B. H., Gaillardet, J., Peucker-ehrenbrink, B., Fischer, W. W., Mcclelland, J. W., Spencer, R. G. M., Voss, B. M., and Adkins, J. F.: Sulfur isotopes in rivers : Insights into global weathering budgets , pyrite oxidation , and the modern sulfur cycle, 496, 168–177, https://doi.org/10.1016/j.epsl.2018.05.022, 2018.

Burke, A., Moore, K. A., Sigl, M., Nita, D. C., Mcconnell, J. R., and Adkins, J. F.: Stratospheric eruptions from tropical and extra-tropical volcanoes constrained using high-resolution sulfur isotopes in ice cores, Earth Planet. Sci. Lett., 521, 113–119,
480   https://doi.org/10.1016/j.epsl.2019.06.006, 2019.

Chen, S., Wang, Y., Cheng, H., Edwards, R. L., Wang, X., Kong, X., and Liu, D.: Strong coupling of Asian Monsoon and Antarctic climates on sub- orbital timescales, Sci. Rep., 6, https://doi.org/10.1038/srep32995, 2016.

Chesner, C. A.: The Toba Caldera Complex, Quat. Int., 258, 5–18, https://doi.org/10.1016/j.quaint.2011.09.025, 2012.

Chesner, C. A. and Luhr, J. F.: A melt inclusion study of the Toba Tuffs , Sumatra , Indonesia, J. Volcanol. Geotherm. Res.,
485   197, 259–278, https://doi.org/10.1016/j.jvolgeores.2010.06.001, 2010.

Chesner, C. A., Rose, W. I., Deino, A., Drake, R., and Westgate, J. A.: Eruptive history of Earth's largest Quaternary caldera

(Toba, Indonesia) clarified, Geology, 19, 200, https://doi.org/10.1130/0091-7613(1991)019<0200:EHOESL>2.3.CO;2, 1991.

Clarkson, C., Harris, C., Li, B., Neudorf, C. M., Roberts, R. G., Lane, C., Norman, K., Pal, J., Jones, S., Shipton, C., Koshy, J., Gupta, M. C., Mishra, D. P., Dubey, A. K., Boivin, N., and Petraglia, M.: Human occupation of northern India spans the

490   Toba super-eruption ~74,000 years ago, Nat. Commun., 11, 1–10, https://doi.org/10.1038/s41467-020-14668-4, 2020.

Cole-Dai, J.: Volcanoes and climate, Wiley Interdiscip. Rev. Clim. Chang., 1, 824–839, https://doi.org/10.1002/wcc.76, 2010.

Cole-Dai, J., Ferris, D., Lanciki, A., Savarino, J., Baroni, M., and Thiemens, M. H.: Cold decade (AD 1810-1819) caused by Tambora (1815) and another (1809) stratospheric volcanic eruption, Geophys. Res. Lett., 36, 1–6, https://doi.org/10.1029/2009GL040882, 2009.

495   Costa, A., Smith, V. C., Macedonio, G., and Matthews, N. E.: The magnitude and impact of the Youngest Toba Tuff super-eruption, Front. Earth Sci., 2, 1–8, https://doi.org/10.3389/feart.2014.00016, 2014.

Costa, A., Suzuki, Y. J., Cerminara, M., Devenish, B. J., Ongaro, T. E., Herzog, M., Van Eaton, A. R., Denby, L. C., Bursik, M., de' Michieli Vitturi, M., Engwell, S., Neri, A., Barsotti, S., Folch, A., Macedonio, G., Girault, F., Carazzo, G., Tait, S., Kaminski, E., Mastin, L. G., Woodhouse, M. J., Phillips, J. C., Hogg, A. J., Degruyter, W., and Bonadonna, C.: Results of the

500   eruptive column model inter-comparison study, J. Volcanol. Geotherm. Res., 326, 2–25, https://doi.org/10.1016/j.jvolgeores.2016.01.017, 2016.

Costa, A., Suzuki, Y. J., and Koyaguchi, T.: Understanding the plume dynamics of explosive super-eruptions, Nat. Commun., 9, https://doi.org/10.1038/s41467-018-02901-0, 2018.

Druitt, T. H., Costa, F., Deloule, E., Dungan, M., and Scaillet, B.: Decadal to monthly timescales of magma transfer and

505   reservoir growth at a caldera volcano, Nature, 482, 77–80, https://doi.org/10.1038/nature10706, 2012.

Du, W., Cheng, H., Xu, Y., Yang, X., Zhang, P., Sha, L., Li, H., Zhu, X., Zhang, M., Stríkis, N. M., Cruz, F. W., Edwards, R. L., Zhang, H., and Ning, Y.: Timing and structure of the weak Asian Monsoon event about 73,000 years ago, Quat. Geochronol., 53, 101003, https://doi.org/10.1016/j.quageo.2019.05.002, 2019.

Engwell, S. L., Sparks, R. S. J., and Carey, S.: Physical characteristics of tephra layers in the deep sea realm: the Campanian

510   Ignimbrite eruption, https://doi.org/10.1144/SP398.7, 2014.

Engwell, S. L., de' Michieli Vitturi, M., Esposti Ongaro, T., and Neri, A.: Insights into the formation and dynamics of coignimbrite plumes from one-dimensional models, J. Geophys. Res. Solid Earth, 121, 4211–4231, https://doi.org/10.1002/2016JB012793, 2016.

Gao, C., Oman, L., Robock, A., and Stenchikov, G. L.: Atmospheric volcanic loading derived from bipolar ice cores:

515   Accounting for the spatial distribution of volcanic deposition, J. Geophys. Res., 112, https://doi.org/10.1029/2006JD007461, 2007.

Gautier, E., Savarino, J., Erbland, J., Lanciki, A., and Possenti, P.: Variability of sulfate signal in ice core records based on five replicate cores, Clim. Past, 12, 103–113, https://doi.org/10.5194/cp-12-103-2016, 2016.

Gautier, E., Savarino, J., Erbland, J., and Farquhar, J.: SO2 Oxidation Kinetics Leave a Consistent Isotopic Imprint on Volcanic

520   Ice Core Sulfate, J. Geophys. Res. Atmos., 123, 9801–9812, https://doi.org/10.1029/2018JD028456, 2018.

Gautier, E., Savarino, J., Hoek, J., Erbland, J., Caillon, N., Hattori, S., Albarede, F., Farquhar, J., and Yoshida, N.: 2600-years of stratospheric volcanism through sulfate isotopes, Nat. Commun., 10, 1–7, https://doi.org/10.1038/s41467-019-08357-0, 2019.

Guo, S., Bluth, G. J. S., Rose, W. I., Watson, I. M., and Prata, A. J.: Re-evaluation of SO2 release of the 15 June 1991 Pinatubo eruption using ultraviolet and infrared satellite sensors, https://doi.org/10.1029/2003GC000654, 2004.

Iverson, N. A., Kalteyer, D., Dunbar, N. W., Kurbatov, A., and Yates, M.: Advancements and best practices for analysis and correlation of tephra and cryptotephra in ice, Quat. Geochronol., 40, 45–55, https://doi.org/10.1016/j.quageo.2016.09.008, 2017.

Kandlbauer, J. and Sparks, R. S. J.: New estimates of the 1815 Tambora eruption volume, J. Volcanol. Geotherm. Res., 286, 93–100, https://doi.org/10.1016/j.jvolgeores.2014.08.020, 2014.

Kandlbauer, J., Carey, S. N., and Sparks, R. S. J.: The 1815 Tambora ash fall : implications for transport and deposition of distal ash on land and in the deep sea, Bull. Volcanol., 75, 708–718, https://doi.org/10.1007/s00445-013-0708-3, 2013.

Kindler, P., Guillevic, M., Baumgartner, M., Schwander, J., Landais, A., and Leuenberger, M.: Temperature reconstruction from 10 to 120 kyr b2k from the NGRIP ice core, Clim. Past, 10, 887–902, https://doi.org/10.5194/cp-10-887-2014, 2014.

Lane, C. S., Chorn, B. T., and Johnson, T. C.: Ash from the Toba supereruption in Lake Malawi shows no volcanic winter in East Africa at 75 ka, Proc. Natl. Acad. Sci. U. S. A., 110, 8025–8029, https://doi.org/10.1073/pnas.1301474110, 2013.

Lavigne, F., Degeai, J.-P., Komorowski, J.-C., Guillet, S., Robert, V., Lahitte, P., Oppenheimer, C., Stoffel, M., Vidal, C. M., Surono, Pratomo, I., Wassmer, P., Hajdas, I., Hadmoko, D. S., and de Belizal, E.: Source of the great A.D. 1257 mystery eruption unveiled, Samalas volcano, Rinjani Volcanic Complex, Indonesia, Proc. Natl. Acad. Sci., 110, 16742–16747, https://doi.org/10.1073/pnas.1307520110, 2013.

Liang, X., Wei, G., Shao, L., Li, X., and Wang, R.: Records of Toba eruptions in the South China Sea, Sci. China Ser. D Earth Sci., 44, 871–878, https://doi.org/10.1007/BF02907078, 2001.

Lin, M., Zhang, X., Li, M., Xu, Y., Zhang, Z., Tao, J., Su, B., Liu, L., Shen, Y., and Thiemens, M. H.: Five-S-isotope evidence of two distinct mass-independent sulfur isotope effects and implications for the modern and Archean atmospheres, 115, 8541–8546, https://doi.org/10.1073/pnas.1803420115, 2018.

Mark, D. F., Petraglia, M., Smith, V. C., Morgan, L. E., Barfod, D. N., Ellis, B. S., Pearce, N. J., Pal, J. N., and Korisettar, R.: A high-precision 40 Ar / 39 Ar age for the Young Toba Tuff and dating of ultra-distal tephra : Forcing of Quaternary climate and implications for hominin occupation of India, Quat. Geochronol., 21, 90–103, https://doi.org/10.1016/j.quageo.2012.12.004, 2014.

Mark, D. F., Renne, P. R., Dymock, R., Smith, V. C., Simon, J. I., Morgan, L. E., Staff, R. A., and Ellis, B. S.: High-precision 40Ar/39Ar dating of pleistocene tuffs and temporal anchoring of the Matuyama-Brunhes boundary, Quat. Geochronol., 39, 1–23, https://doi.org/10.1016/j.quageo.2017.01.002, 2017.

McConnell, J. R., Burke, A., Dunbar, N. W., Köhler, P., Thomas, J. L., Arienzo, M. M., Chellman, N. J., Maselli, O. J., Sigl, M., Adkins, J. F., Baggenstos, D., Burkhart, J. F., Brook, E. J., Buizert, C., Cole-Dai, J., Fudge, T. J., Knorr, G., Graf, H.-F.,

555   Grieman, M. M., Iverson, N., McGwire, K. C., Mulvaney, R., Paris, G., Rhodes, R. H., Saltzman, E. S., Severinghaus, J. P., Steffensen, J. P., Taylor, K. C., and Winckler, G.: Synchronous volcanic eruptions and abrupt climate change ~17.7 ka plausibly linked by stratospheric ozone depletion, 114, 10035–10040, https://doi.org/10.1073/pnas.1705595114, 2017.

Narcisi, B., Petit, J. R., Delmonte, B., Batanova, V., and Savarino, J.: Multiple sources for tephra from AD 1259 volcanic signal in Antarctic ice cores, Quat. Sci. Rev., 210, 164–174, https://doi.org/10.1016/j.quascirev.2019.03.005, 2019.

560   Ninkovich, D., Sparks, R. S. J., and Ledbetter, M. T.: The exceptional magnitude and intensity of the Toba eruption , Sumatra: An example of the use of deep-sea tephra layers as a geological tool, Bull. Volcanol., 41, 286–298, https://doi.org/10.1007/BF02597228, 1978.

Oppenheimer, C.: Limited global change due to the largest known Quaternary eruption , Toba 74 kyr BP ?, Quat. Sci. Rev., 21, 1593–1609, https://doi.org/https://doi.org/10.1016/S0277-3791(01)00154-8, 2002.

565   Paris, G., Sessions, A. L., Subhas, A. V, and Adkins, J. F.: MC-ICP-MS measurement of delta S-34 and Delta S-33 in small amounts of dissolved sulfate, https://doi.org/https://doi.org/10.1016/j.chemgeo.2013.02.022, 2013.

Petraglia, M. D., Ditchfield, P., Jones, S., Korisettar, R., and Pal, J. N.: The Toba volcanic super-eruption, environmental change, and hominin occupation history in India over the last 140,000 years, Quat. Int., 258, 119–134, https://doi.org/10.1016/j.quaint.2011.07.042, 2012.

570   Polyak, V. J., Asmerom, Y., and Lachniet, M. S.: Rapid speleothem δ 13 C change in southwestern North America coincident with Greenland stadial 20 and the Toba (Indonesia) supereruption, Geology, 45, 843–846, https://doi.org/10.1130/G39149.1, 2017.

Rampino, M. R. and Ambrose, S. H.: Volcanic winter in the Garden of Eden : The Toba supereruption and the late Pleistocene human population crash, Geol. Soc. Am., 345, 71–82, https://doi.org/10.1130/0-8137-2345-0.71, 2000.

575   Rasmussen, S. O., Bigler, M., Blockley, S. P., Blunier, T., Buchardt, S. L., Clausen, H. B., Cvijanovic, I., Dahl-Jensen, D., Johnsen, S. J., Fischer, H., Gkinis, V., Guillevic, M., Hoek, W. Z., Lowe, J. J., Pedro, J. B., Popp, T., Seierstad, I. K., Steffensen, J. P., Svensson, A. M., Vallelonga, P., Vinther, B. M., Walker, M. J. C., Wheatley, J. J., and Winstrup, M.: A stratigraphic framework for abrupt climatic changes during the Last Glacial period based on three synchronized Greenland ice-core records: Refining and extending the INTIMATE event stratigraphy, Quat. Sci. Rev., 106, 14–28,

580   https://doi.org/10.1016/j.quascirev.2014.09.007, 2014.

Robock, A.: Volcanic eruptions and climate, Rev. Geophys., 38, 191–219, https://doi.org/https://doi.org/10.1029/1998RG000054, 2000.

Rougier, J., Sparks, R. S. J., Cashman, K. V., and Brown, S. K.: The global magnitude–frequency relationship for large explosive volcanic eruptions, Earth Planet. Sci. Lett., 482, 621–629, https://doi.org/10.1016/j.epsl.2017.11.015, 2018.

585   Savarino, J., Romero, A., Cole-Dai, J., Bekki, S., and Thiemens, M. H.: UV induced mass-independent sulfur isotope fractionation in stratospheric volcanic sulfate, Geophys. Res. Lett., 30, 2131, https://doi.org/10.1029/2003GL018134, 2003.

Self, S. and Rampino, M. R.: The 1963-1964 eruption of Agung volcano (Bali, Indonesia), Bull. Volcanol., 74, 1521–1536, https://doi.org/10.1007/s00445-012-0615-z, 2012.

Severi, M., Becagli, S., Castellano, E., Morganti, A., Traversi, R., Udisti, R., Ruth, U., Fischer, H., and Huybrechts, P.:
590   Synchronisation of the EDML and EDC ice cores for the last 52 kyr by volcanic signature matching, Clim. Past, 3, 367–374,
https://doi.org/https://doi.org/10.5194/cp-3-367-2007, 2007.

Shaheen, R., Abauanza, M., Jackson, T. L., McCabe, J., Savarino, J., and Thiemens, M. H.: Tales of volcanoes and El-Nino
southern oscillations with the oxygen isotope anomaly of sulfate aerosol., Proc. Natl. Acad. Sci. U. S. A., 110, 17662–7,
https://doi.org/10.1073/pnas.1213149110, 2013.

595   Shamloo, H. I. and Till, C. B.: Decadal transition from quiescence to supereruption: petrologic investigation of the Lava Creek
Tuff, Yellowstone Caldera, WY, Contrib. to Mineral. Petrol., 174, 32, https://doi.org/10.1007/s00410-019-1570-x, 2019.

Sigl, M., McConnell, J. R., Layman, L., Maselli, O., McGwire, K., Pasteris, D., Dahl-Jensen, D., Steffensen, J. P., Vinther, B.,
Edwards, R., Mulvaney, R., and Kipfstuhl, S.: A new bipolar ice core record of volcanism from WAIS Divide and NEEM and
implications   for   climate   forcing   of   the   last   2000   years,   J.   Geophys.   Res.   Atmos.,   118,   1151–1169,
600   https://doi.org/10.1029/2012JD018603, 2013.

Sigl, M., Winstrup, M., McConnell, J. R., Welten, K. C., Plunkett, G., Ludlow, F., Büntgen, U., Caffee, M., Chellman, N.,
Dahl-Jensen, D., Fischer, H., Kipfstuhl, S., Kostick, C., Maselli, O. J., Mekhaldi, F., Mulvaney, R., Muscheler, R., Pasteris,
D. R., Pilcher, J. R., Salzer, M., Schüpbach, S., Steffensen, J. P., Vinther, B. M., and Woodruff, T. E.: Timing and climate
forcing of volcanic eruptions for the past 2,500 years., Nature, 523, 543–9, https://doi.org/https://doi.org/10.1038/nature14565,
605   2015.

Sigurdsson, H. and Carey, S.: Plinian and co-ignimbrite tephra fall from the the 1815 eruption of Tambora volcano, Bull.
Volcanol., 51, 243–270, https://doi.org/10.1007/BF01073515, 1989.

Smith, E. I., Jacobs, Z., Johnsen, R., Ren, M., Fisher, E. C., Oestmo, S., Wilkins, J., Harris, J. A., Karkanas, P., Fitch, S.,
Ciravolo, A., Keenan, D., Cleghorn, N., Lane, C. S., Matthews, T., and Marean, C. W.: Humans thrived in South Africa through
610   the Toba eruption about 74,000 years ago, Nature, 555, 511–515, https://doi.org/10.1038/nature25967, 2018.

Sparks, R. S. J., Brown, S. K., Burke, A., Crick, L., Doyle, E. A., Innes, H. M., Mahony, S., Rae, J. W. B., Rougier, J. C.,
Severi, M., and Wolff, E. W.: Steady state large magnitude explosive volcanism for the last five hundred thousand years (in
review), n.d.

Storey, M., Roberts, R. G., and Saidin, M.: Astronomically calibrated 40Ar/39Ar age for the Toba supereruption and global
615   synchronization   of   late   Quaternary   records,   Proc.   Natl.   Acad.   Sci.   U.   S.   A.,   109,   18684–18688,
https://doi.org/10.1073/pnas.1208178109, 2012.

Svensson, A., Bigler, M., Blunier, T., Clausen, H. B., Dahl-Jensen, D., Fischer, H., Fujita, S., Goto-Azuma, K., Johnsen, S. J.,
Kawamura, K., Kipfstuhl, S., Kohno, M., Parrenin, F., Popp, T., Rasmussen, S. O., Schwander, J., Seierstad, I., Severi, M.,
Steffensen, J. P., Udisti, R., Uemura, R., Vallelonga, P., Vinther, B. M., Wegner, A., Wilhelms, F., and Winstrup, M.: Direct
620   linking of Greenland and Antarctic ice cores at the Toba eruption (74 ka BP), Clim. Past, 9, 749–766,
https://doi.org/10.5194/cp-9-749-2013, 2013.

Swallow, E. J., Wilson, C. J. N., Charlier, B. L. A., and Gamble, J. A.: The Huckleberry Ridge Tuff, Yellowstone: Evacuation

of multiple magmatic systems in a complex episodic eruption, J. Petrol., 60, 1371–1426, https://doi.org/10.1093/petrology/egz034, 2019.

625 Toohey, M. and Sigl, M.: Volcanic stratospheric sulfur injections and aerosol optical depth from 500BCE to 1900CE, Earth Syst. Sci. Data, 9, 809–831, https://doi.org/10.1108/eb058541, 2017.

Toohey, M., Krüger, K., Sigl, M., Stordal, F., and Svensen, H.: Climatic and societal impacts of a volcanic double event at the dawn of the Middle Ages, Clim. Change, 136, 401–412, https://doi.org/10.1007/s10584-016-1648-7, 2016.

Toohey, M., Krüger, K., Schmidt, H., Timmreck, C., Sigl, M., Stoffel, M., and Wilson, R.: Disproportionately strong climate
630 forcing from extratropical explosive volcanic eruptions, Nat. Geosci., 12, 100–107, https://doi.org/10.1038/s41561-018-0286-2, 2019.

Veres, D., Bazin, L., Landais, A., Toyé Mahamadou Kele, H., Lemieux-Dudon, B., Parrenin, F., Martinerie, P., Blayo, E., Blunier, T., Capron, E., Chappellaz, J., Rasmussen, S. O., Severi, M., Svensson, A., Vinther, B., and Wolff, E. W.: The Antarctic ice core chronology (AICC2012): An optimized multi-parameter and multi-site dating approach for the last 120
635 thousand years, Clim. Past, 9, 1733–1748, https://doi.org/10.5194/cp-9-1733-2013, 2013.

Vidal, C. M., Métrich, N., Komorowski, J. C., Pratomo, I., Michel, A., Kartadinata, N., Robert, V., and Lavigne, F.: The 1257 Samalas eruption (Lombok, Indonesia): The single greatest stratospheric gas release of the Common Era, Sci. Rep., 6, 1–13, https://doi.org/10.1038/srep34868, 2016.

Wang, Y. J., Cheng, H., Edwards, R. L., An, Z. S., Wu, J. Y., Shen, C. C., and Dorale, J. A.: A high-resolution absolute-dated
640 late pleistocene monsoon record from Hulu Cave, China, Science, 294, 2345–2348, https://doi.org/10.1126/science.1064618, 2001.

Williams, M.: The ~73 ka Toba super-eruption and its impact: History of a debate, Quat. Int., 258, 19–29, https://doi.org/10.1016/j.quaint.2011.08.025, 2012.

Wilson, C. J. N.: Supereruptions and Supervolcanoes: Processes and Products, 4, 29–34,
645 https://doi.org/10.2113/GSELEMENTS.4.1.29, 2008.

Wolff, E. W., Barbante, C., Becagli, S., Bigler, M., Boutron, C. F., Castellano, E., de Angelis, M., Federer, U., Fischer, H., Fundel, F., Hansson, M., Hutterli, M., Jonsell, U., Karlin, T., Kaufmann, P., Lambert, F., Littot, G. C., Mulvaney, R., Röthlisberger, R., Ruth, U., Severi, M., Siggaard-Andersen, M. L., Sime, L. C., Steffensen, J. P., Stocker, T. F., Traversi, R., Twarloh, B., Udisti, R., Wagenbach, D., and Wegner, A.: Changes in environment over the last 800,000 years from chemical
650 analysis of the EPICA Dome C ice core, Quat. Sci. Rev., 29, 285–295, https://doi.org/10.1016/j.quascirev.2009.06.013, 2010a.

Wolff, E. W., Chappellaz, J., Blunier, T., Rasmussen, S. O., and Svensson, A.: Millennial-scale variability during the last glacial: The ice core record, Quat. Sci. Rev., 29, 2828–2838, https://doi.org/10.1016/j.quascirev.2009.10.013, 2010b.

York, D., Evensen, N. M., Martínez, M. L., and De Basabe Delgado, J.: Unified equations for the slope, intercept, and standard errors of the best straight line, Am. J. Phys., 72, 367–375, https://doi.org/10.1119/1.1632486, 2004.

655 Yost, C. L., Jackson, L. J., Stone, J. R., and Cohen, A. S.: Subdecadal phytolith and charcoal records from Lake Malawi, East Africa imply minimal effects on human evolution from the ~74 ka Toba supereruption, J. Hum. Evol., 116, 75–94,

https://doi.org/https://doi.org/10.1016/j.jhevol.2017.11.005, 2018.

Zahn, A., Franz, P., Bechtel, C., Grooß, J. U., and Röckmann, T.: Modelling the budget of middle atmospheric water vapour isotopes, Atmos. Chem. Phys., 6, 2073–2090, https://doi.org/10.5194/acp-6-2073-2006, 2006.

660   Zielinski, G. A.: Use of paleo-records in determining variability within the volcanism-climate system, Quat. Sci. Rev., 19, 417–438, https://doi.org/https://doi.org/10.1016/S0277-3791(99)00073-6, 2000.

Zielinski, G. A., Mayewski, P. A., Meeker, L. D., Whitlow, S., and Twickler, M. S.: Potential atmospheric impact of the Toba mega-eruption ~ 71,000 years ago, Geophys. Res. Lett., 23, 837–840, https://doi.org/https://doi.org/10.1029/96GL00706, 1996.

665
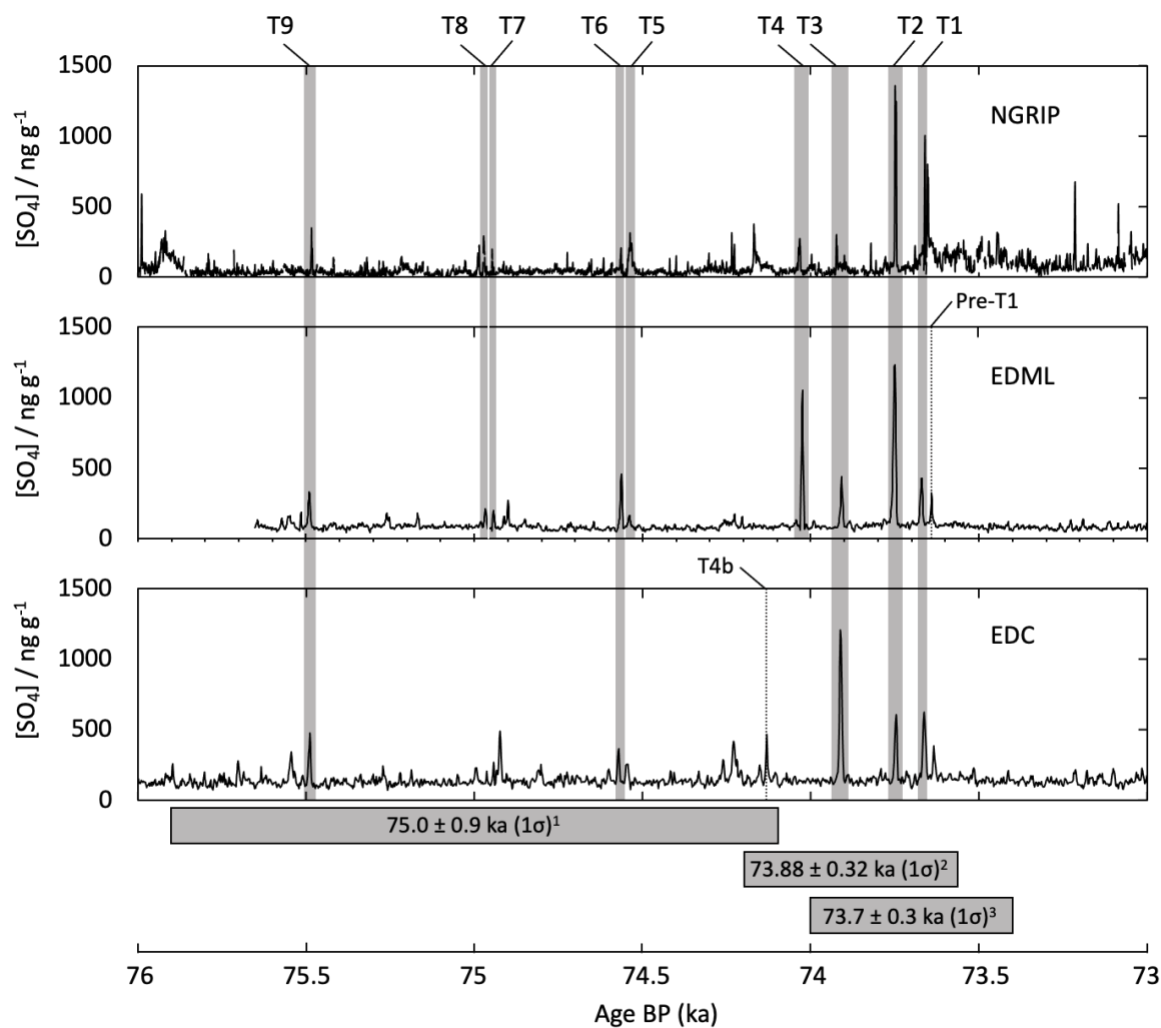
Figure 1. Toba candidates identified in both Greenland (NGRIP) and Antarctic (EDML, EDC) ice cores by Svensson et al., (2013). Sulfate concentration data from Svensson et al., (2013) [NGRIP and EDML] and Sparks et al., (in review) [EDC]. The AICC2012 ice core chronology (Bazin et al., 2013; Veres et al., 2013) was applied to both Greenland and Antarctic ice cores. Dotted lines indicate the additional peaks measured in EDC and EDML. The age estimates for the Toba eruption from 1) Mark et al., (2014), 2) Storey et al., (2012) and 3) Mark et al., (2017) are represented by horizontal bars indicating 1σ for each date. Note that the stated uncertainty in AICC2012 dates at this period is around 1500 years.

Climate
of the Past
Discussions
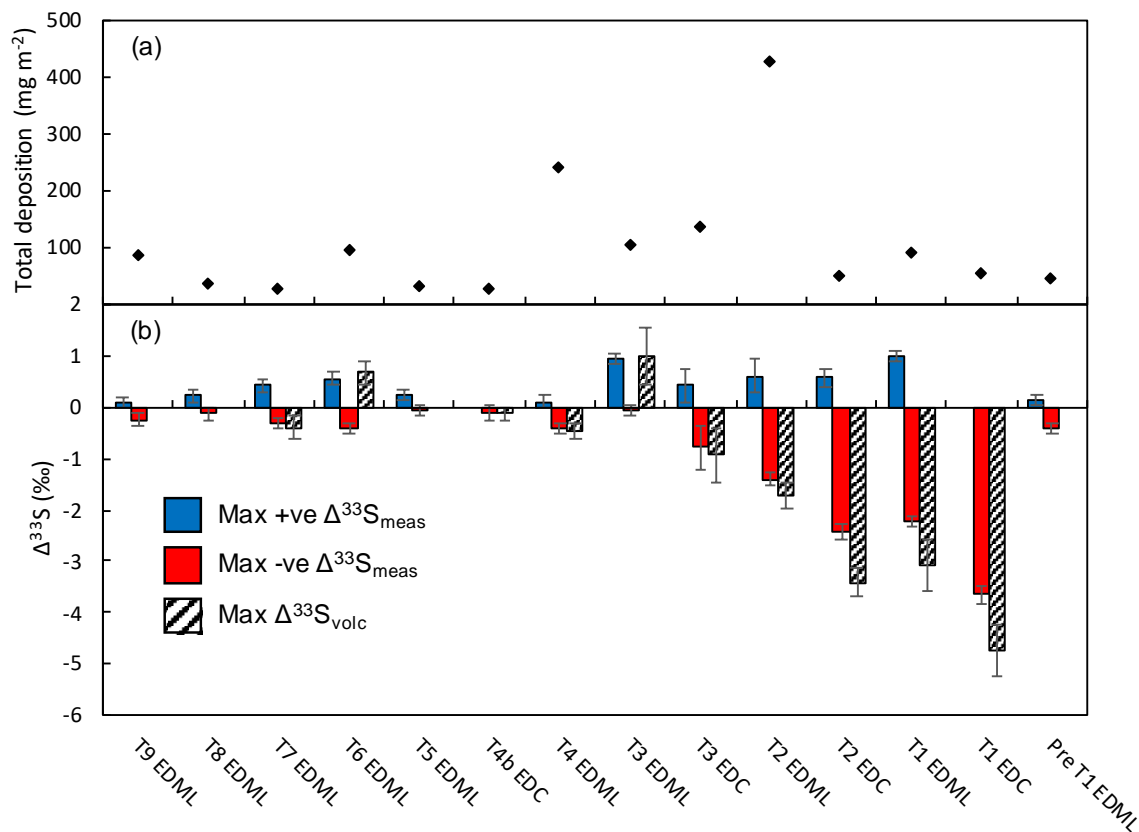
Figure 2. Total deposition and $\Delta^{33}S$ data for the 14 Toba candidate peaks. 2a) shows total deposition for each peak. 2b) Filled bars show the maximum positive and negative fractionations measured. Patterned bars indicate the maximum magnitude $\Delta^{33}S_{volc}$ determined by isotopic mass balance for each peak with samples with $f_{volc} \geq 0.65$, one data point from T3 in EDML with $f_{volc} = 0.63$ has also been included. 2σ errors have been included for $\Delta^{33}S_{meas}$ data and propagated 1σ errors for $\Delta^{33}S_{volc}$.
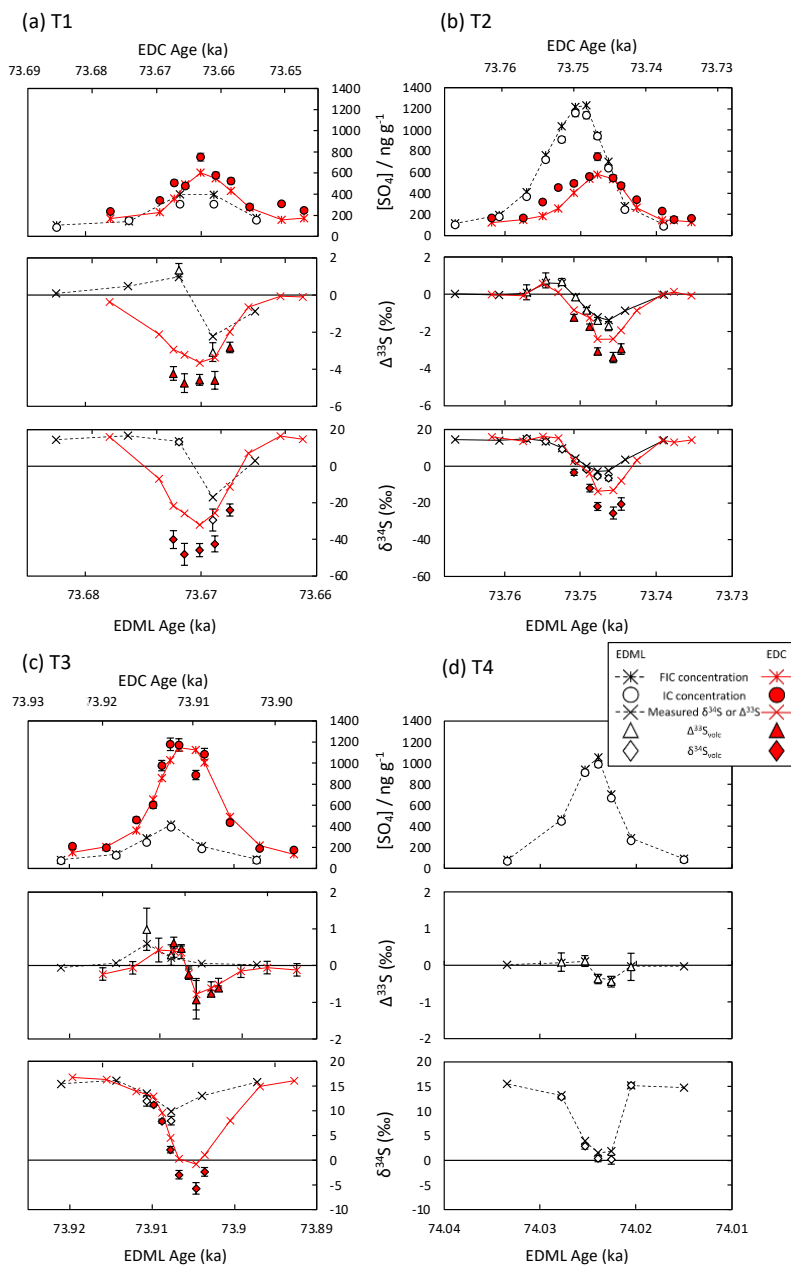
Figure 3. Sulfur isotopes in sulfate from T1, T2, T3 and T4 in both EDC (a–c) and EDML (all). Red lines and filled symbols are data from the EDC ice core and black represents EDML. Both FIC (lines) and IC (points) data have been plotted for concentration. Lines on the isotope plots show measured values and symbols are background corrected data where f$_{volc}$ ≥ 0.65, as well as one point from T3 in EDML with f$_{volc}$ = 0.63. Error bars indicate 2σ for measured ratios and 1σ for background corrected ratios, where error bars are not visible the error is smaller than the symbol. Peaks have been aligned visually based on the isotope records, and this results in minor (<15 y) differences in the AICC2012 age model alignment between the two cores. Note the different scale for the isotopic data in c and d compared to a and b.

685
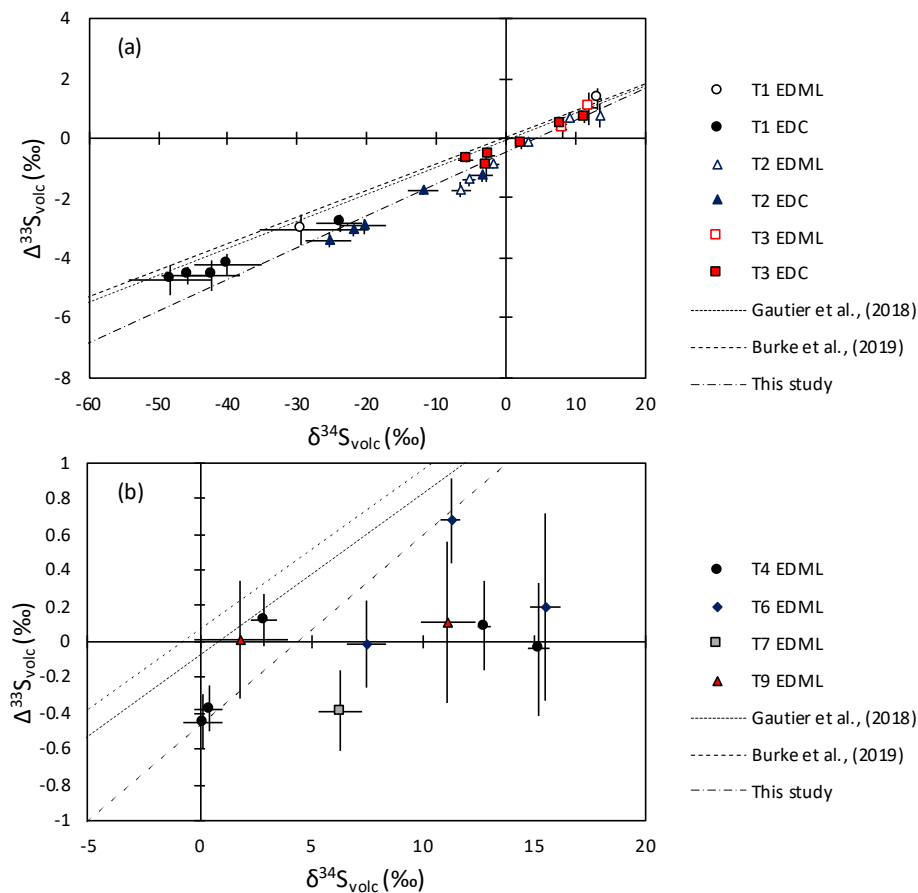
Figure 4. Δ³³S_volc and δ³⁴S_volc for Toba candidates in EDC and EDML. a) Candidates that show a positive correlation indicative of purely stratospheric sulfate, also plotted are linear York regression (York et al., 2004) of the low-latitude stratospheric data (T1–T3) and the regressions from Gautier et al., (2018) and known tropical eruptions from Burke et al., (2019). b) Extratropical candidates with no correlation.
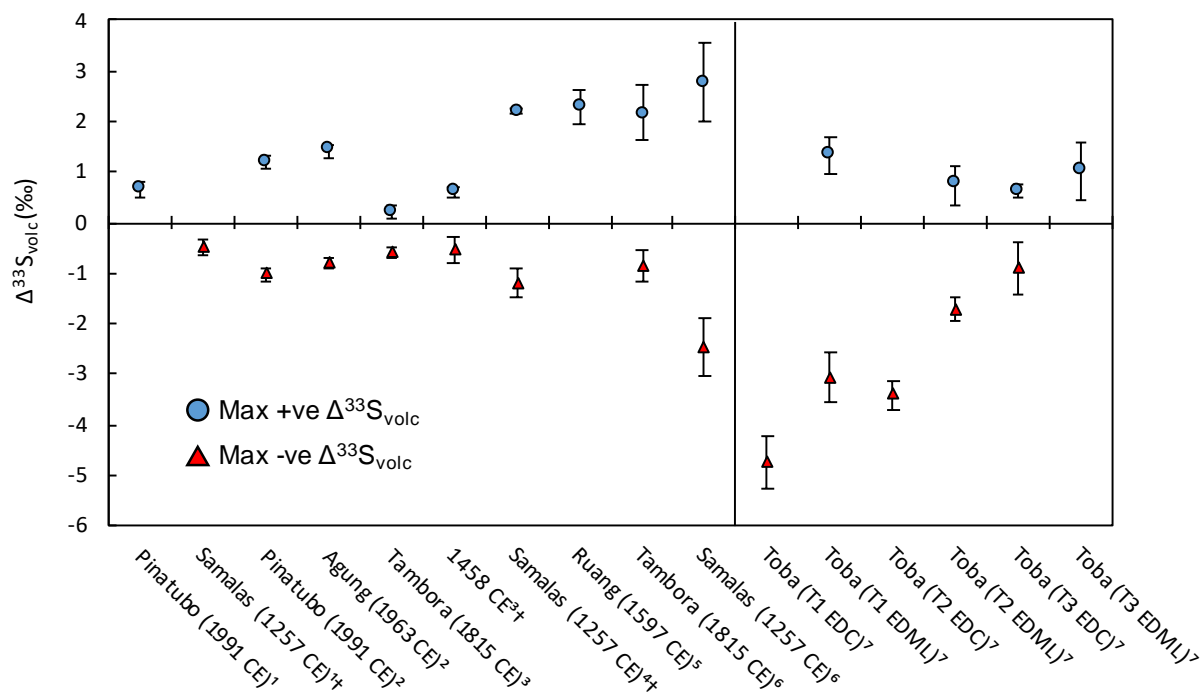
Figure 5. Comparison between $\Delta^{33}S_{volc}$ measured for volcanic events in this study and the largest volcanic S-MIF from previous studies of historical eruptions. Data sources: 1) Savarino et al., (2003), 2) Baroni et al., (2007), 3) Cole-Dai et al., (2009), 4) Gautier et al., (2018), 5) Gautier et al., (2019), 6) Burke et al., (2019), 7) This study. †These dates are taken from Sigl et al., (2015).
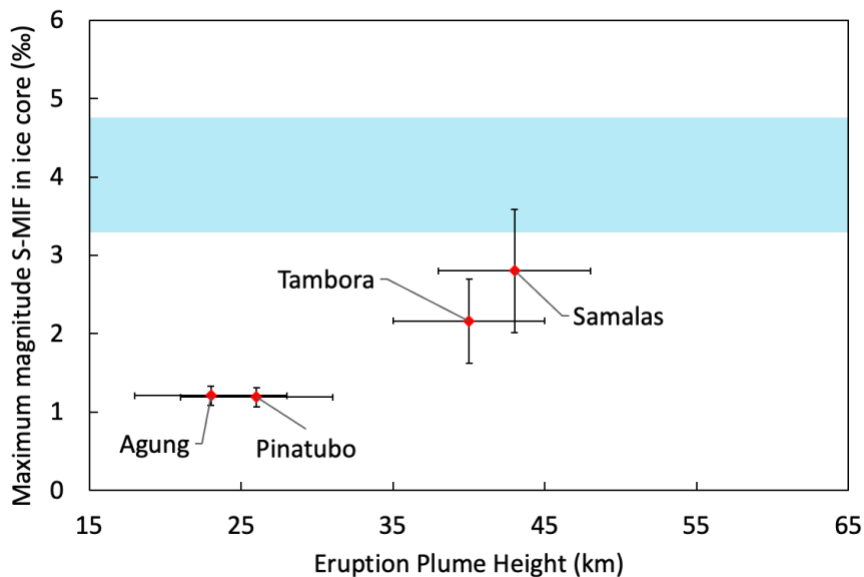
Figure 6. Maximum S-MIF signal ($\Delta^{33}S$) versus eruptive plume height for Common Era events. Highlighted box indicates the region of T1 and T2 MIF signals from this study. Height estimates are from Self and Rampino, 2012 (Agung), Guo et al., 2004 (Pinatubo), Kandlbauer and Sparks, 2014 (Tambora) and Vidal et al., 2016 (Samalas). $\Delta^{33}S$ data are from Baroni et al., 2007 (Pinatubo, Agung) and Burke et al., 2019 (Tambora, Samalas)
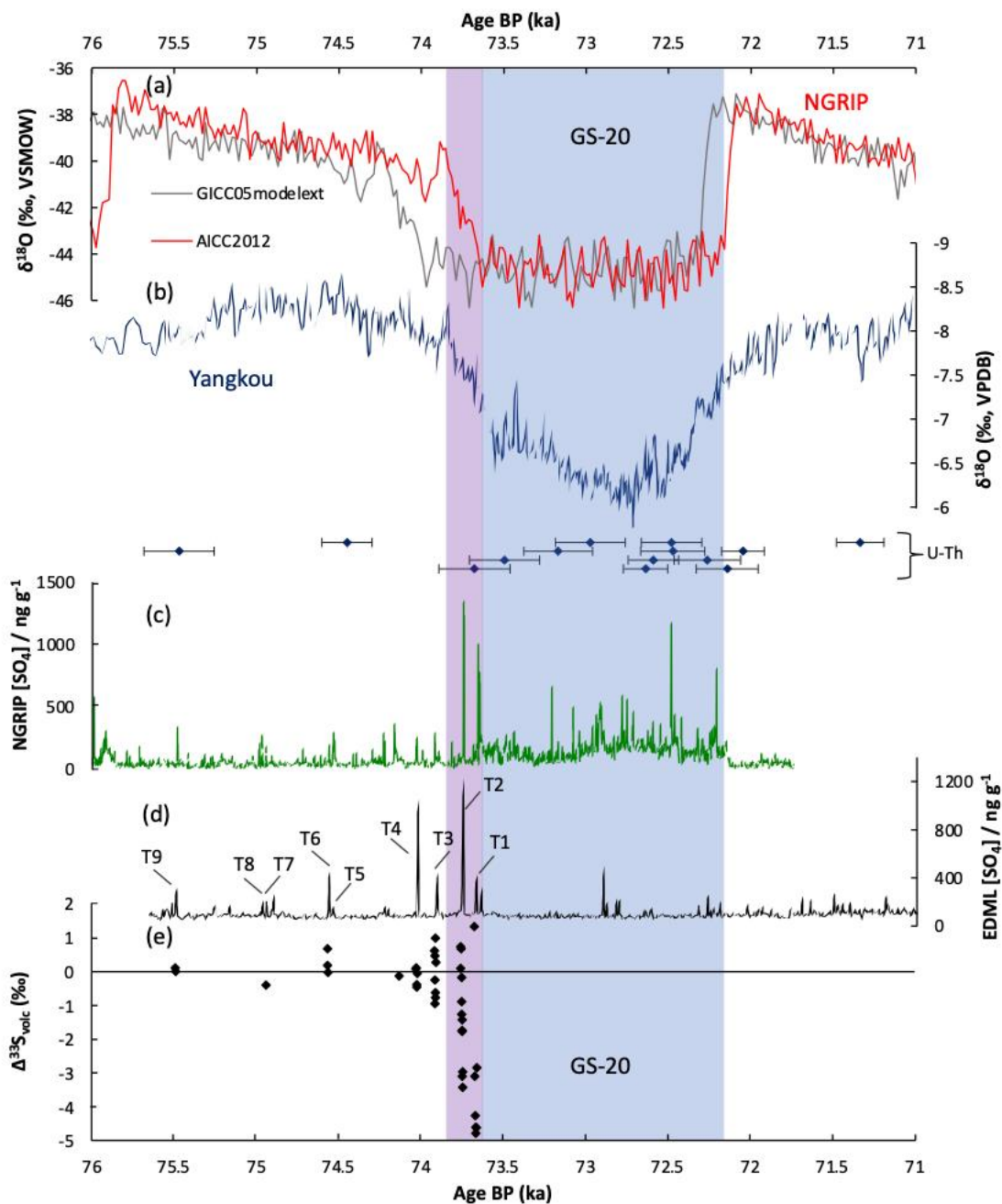
Figure 7. Paleoclimate indicators across GS-20 (highlighted in blue based upon NGRIP δ18O with the transition in purple). All ice core data is plotted using the AICC2012 age model unless indicated otherwise. a) Ice core oxygen isotope data from NGRIP (Buizert et al., 2015) on both the AICC2012 age model (red) and GICC05modelext age model (Wolff et al., 2010b) (grey) ; b) δ18O speleothem records from Yangkou, China; the U-Th age data for Yangkou has also been included (blue diamonds) along with their associated 2σ error (Du et al., 2019); c) continuous sulfate concentration in NGRIP and EDML (d) (Svensson et al., 2013); e) Δ^{33}S$_{volc}$ measured for Toba candidates in this study.